Thermography for Monitoring the Selective Laser Melting Process

H. Krauss*, C. Eschey*, M. F. Zaeh*
*Institute for Machine Tools and Industrial Management (*iwb*), Technische Universitaet
Muenchen, Germany

Abstract

A lot of strategies exist to monitor and control additive layer manufacturing processes. Basically one can distinguish between coaxially monitoring the process zone and monitoring the complete layer currently being built. Since Selective Laser Melting is a thermal process, a lot of information about the process and in consequence about the resulting part quality can be gathered by monitoring the temperature distribution of a complete layer and its temporal evolution. It depends on the geometrical configuration of parts being built and the quality of the powder layer deposition. In this paper, process errors originating from insufficient heat dissipation are investigated as well as the limits for detecting pores and other irregularities by observation of the temperature distribution.

Introduction

Today additive manufacturing technologies are in a transition phase from research to industrial applications. The economic manufacturing of small to medium lot sizes as well as the achievable part properties put this technology in the role of a promising alternative to conventional manufacturing processes [1]. Regarding the serial production of safety-related components for example in automotive or aeronautic applications, the detailed documentation of the part quality becomes increasingly important. This can be done by different means including the manufacturing of ancillary test specimens or the non-destructive testing using computer tomography. In contrast to subsequent part testing the layerwise build up process in additive manufacturing allows for detailed monitoring of the whole components currently being manufactured within the process.

Laser processes are mostly thermal processes, giving rise for thermal or near IR monitoring [2], which is subject of this paper. Using a spatially resolving detector in contrast to a spatially integrating sensor, for example an infrared diode, has the advantage of being able to do a geometrical characterization of the process zone and in general of the heat affected zone.

Process monitoring will be of great importance for demanding applications, but should be realizable with a reasonable cost-benefit ratio in order to help spreading the promising technology of additive layer manufacturing (ALM). Therefore the system for investigating the heat affected zone chosen here is an infrared camera of medium spatial and temporal resolution. The potentials and drawbacks of thermography measurements implying cost efficient radiation sensors (bolometer detector) shall be analyzed for ALM of metallic parts.

State of the art

Process monitoring and surveillance is a common method for documenting process conditions and process results in laser based manufacturing. The detection systems employed depend on specific requirements of the applications ranging from ultrasonic and acoustic to optical and

thermal sensors. For ALM a coaxial setup was developed by [3] which focused on monitoring the irradiance emitted by the melt pool. Since the setup uses the same scanning unit for material processing and process monitoring, the detector elements are always focused on the current process zone. Since the commonly used optical elements for laser guidance and deflection are optimized for a small spectral region around the laser wavelength, this setup only allows for monitoring radiation close to this wavelength. The system implies a spatially integrating photodiode and a spatially resolving CMOS detector for measuring the melt pool radiance which is previously filtered by a $0.7\,\mu m - 0.9\,\mu m$ band pass filter. Using field programmable gate arrays, data acquisition for melt pool radiance and data processing at rates of up to 10 kHz are feasible and an optical resolution in the micrometer-range (CMOS-camera) is realized. The total melt pool area as well as the length-to-width ratio, the latter being determined after image tresholding, is identified to be the relevant detection variable when analyzing process errors. Furthermore coating errors originating from severe blade wear can be detected by using a commercially available video camera, which is mounted in the building chamber, and additional illumination sources [4]. Against the background of process controlling at real-time speed, a commercial implementation of this system is currently under development [5, 6, 7]. In [8] the optical setup of a coaxially monitoring system, which will be used in future Selective Laser Melting (SLM) applications, is described. High temporal resolution can be achieved by implementing a coaxially mounted additional illumination laser.

Another approach for monitoring the SLM process is described in [9]. An infrared camera operating at 2.0 kHz - 3.5 kHz in the MWIR[1] wavelength band and a pyrometer in the NIR[2] region are mounted in the building chamber. Regarding brightness temperature, pyrometer measurements showed a clear dependency on increasing layer thickness and hatch distance, which were varied by a factor 10 and a factor 2 respectively. With infrared camera measurements at a spatial resolution of 100 µm per detector pixel, the droplet formation in processing stainless steel 904L powder could be seen. The size and speed of the droplets and sputter particles were determined. Since the setup is off-axial regarding the laser beam and no additional scanning system was employed, only a small part of the building area could be monitored. Furthermore, the relation between the brightness temperature and the real temperature cannot be given. In [10] this setup is modified to feature a two-color pyrometer and a CCD-camera which are coaxially mounted. As described previously the usable wavelength band is severely restricted to a small band around the laser wavelength because the same optics have to be employed. Facing the inadequacies in determining the spatial distribution with a CCD-camera due to image shift problems, the authors conclude that the measurement of the maximum surface temperature with a two-color pyrometer is sufficient for most applications. In this case, a high temporal resolution of 50 µs could be achieved. The investigations were done using process parameters which are not state of the art regarding available laser systems and scanning units.

In-Process monitoring is also done in related processes like Selective Laser Sintering (SLS) of plastics or Electron beam melting (EBM) of metals. Arcam, a company which sells EBM manufacturing systems, develops a camera based surveillance tool. The system will feature a custom image evaluation software and an IR camera that is integrated into the building chamber [11]. The achievable resolution and detection limits are unknown. [12] uses a low resolution IR-camera to investigate the EBM process as well. Due to metallization by metal evaporation, the integrated system is restricted to monitor the current layer only after the solidification process. A

---

[1] Mid-wavelength infrared
[2] Near infrared

shutter is used to protect the equipment during the power input of the electron beam. After the solidification, the system is used to detect flaws which were deliberately introduced by varying the focus diameter. A correlation between the recorded IR images and metallographic pictures could be achieved for defect sizes in the order of the spatial resolution of the employed system, which is 830 μm per pixel. The flaws could be distinguished from properly solidified areas because of different emissivity values for consolidated material and loose powder.

In SLS of plastics, thermography is employed for analyzing the preheated powder bed. [13] characterizes two different radiant heaters used in identical SLS machines in terms of spatial distribution and mean temperature for different heating cycles. Additionally the resulting temperature distribution on the powder bed surface is measured for different build heights. The melt's temperature during the process is determined for different laser power values, scan vector lengths, hatch distances and scan velocities. The melt temperature in this SLS application is in the range of 200 °C to 300 °C and was measured using a 320x240 pixel IR camera with a maximum frame rate of 700 Hz. The authors conclude that in principle it is possible to use thermography for initial operation, service and potentially for process monitoring in SLS applications [14]. Approaches for using thermal imaging in SLS are also developed by systems manufacturers. [15] uses a thermal imaging system for temperature control purposes during the build-up process while [16] employs thermography for checking the quality of powder layer deposition and the quality of already solidified areas in SLS. Investigations on monitoring of related laser material processing applications can be found in [17, 18, 19, 20].

The evolution of the temperature distribution and thermal conductivity in SLM is simulated by [21]. The authors find good correlation to a heat conductivity model by IR imaging of the process at the MWIR wavelength band. Measurements were done at a resolution of 10 μm per detector pixel and 10 Hz sampling rate while processing titanium powder at low scan velocities. Temperature distribution during the build-up is a key factor for process stability and part quality regarding dimensional accuracy. Modeling of heat sources and different exposure strategies for FEM-based analysis of the SLM-process is done in [22]. [23] calculate the temperature distribution in a single powder layer for Gaussian heat input and different exposure parameters.

Aims

The previously described approaches mainly focus on the detection of material and process inhomogeneities during the building process by characterizing the melt pool in terms of size and maximum emission for a specific wavelength band. In this paper, the possibility of monitoring the SLM process is investigated at the level of the heat affected zone by analyzing its spatial extent and the temporal evolution. The heat affected zone and the cool down characteristic are predominated by the employed scan strategy and the geometrical layout of the parts being built. In this feasibility study, the approach for process monitoring at the level of multiple hatch vectors is verified. It takes place at a spatial extent in the range of 0.1 mm to 1 mm and therefore differs from strategies that monitor the melt pool during the process typically at the spatial extent of the order of 100 microns. Spatially resolved monitoring at the level of multiple hatch lines opens up the possibility for in-process surveillance of a complete layer at a time with cost-efficient detectors. An off-axial setup is used, so there is always a fixed relation between the acquired data and the current position of the heat affected zone for each layer of a part. Uncertainties resulting from back calculation of the laser spot position out of the scan data and the scan head position, which can be done in on-axis setups, are therefore not relevant.

The aim of this paper is the characterization of the heat affected zone for a typical scan strategy and the sensitivity quantification of the measurement setup used for specific variations of the scan parameters. Process and material irregularities, for example close to overhanging structures or part contours, are investigated by characterizing the heat affected zone and comparing it to a stable process. Another aim of this paper is the detection of pores and flaws since they have a significant influence on the mechanical properties of the manufactured parts. This is conducted by introducing artificial flaws consisting of unsolidified areas in test specimens.

Approach

The approach for collecting information about the quality of the parts produced by the SLM process is the monitoring of the heat affected zone and the correlation to the part data and scan strategy information for each layer. All experiments were done on a commercial SLM machine EOS M270 after implementing an off-axially mounted thermography system. The investigated material is Inconel 718, a nickel-based super alloy commonly used in aero engine applications.

SLM is a heat intensive process and the resulting material properties mainly depend on the influence of heat during the build-up process. The heat affected zone consists of the melt pool at temperatures above 1255 °C [24] and an already solidified area at elevated temperatures close to the melt pool. High temperature gradients in the order of 10^4 °C/mm [22] lead to a rapid cool down from melt temperature to the preheating temperature. The resulting microstructure is determined by this cool down process, which in turn is dominated by the scan strategy.

Remelting occurs for subsequent hatch lines and depends on the scan velocity and the scan vector length as well as hatch spacing. Therefore the observation of the complete heat affected zone can be of interest regarding part quality. However, the measurement of this zone cannot be done at visible wavelengths since spectral intensity in this regime rapidly decreases with decreasing surface temperature. Planck's law for blackbody radiation gives rise for monitoring the complete heat affected zone at infrared wavelengths instead of visible wavelengths, since heat radiance as the primary information about the surface temperature is predominantly emitted in the infrared regime. The wavelength of maximum radiance at solidus temperature for the considered material is in the near-infrared regime and moves towards far infrared wavelengths for decreasing temperatures as this is the case for the rest of the heat affected zone. A wide range of different thermography strategies exist, all based on the principle of distinguishing defects and irregularities from the surrounding material due to different heat conductivity, heat capacity or material density [25]. The heat flow in surface-near defect zones will be different compared to the homogenous material leading to characteristic temperature distributions on the surface. However, the detection of irregularities using thermography is limited by a characteristic distance between the irregularities and the observed surface. Defect-induced heat flow disturbance will homogenize across this length and become invisible for the camera. In terms of SLM, thermography measurements using only the heat generated by the solidification process can be classified as passive thermography. The time constant for heat dissipation sets a physical limit to the detection of localized interior irregularities and therefore to the temporal resolution of a monitoring system.

Experimental Setup

The thermal imaging system used for this feasibility study is an uncooled microbolometer detector *Infratec Variocam hr head* with a resolution of 640 x 480 pixels and a frame rate of 50 Hz. The detector is sensible in the LWIR[3] range (8-14 µm) and calibrated for temperatures up to 1700 °C. The 50 mm telephoto lens in combination with the microbolometer focal plane array used in this setup allows for a field of view (FOV) of 18° (horizontal) and 13.5° (vertical). With a close-up focusing option the observation distance could be chosen to be 0.5 m. This corresponds to a spatial resolution of 250 µm per detector pixel and covers an area of surveillance of 160 mm x 120 mm. The total build area of the SLM system is 250 mm x 250 mm while the chosen experimental setup for thermal imaging covers a ratio of 30%. Due to accessibility restrictions, the thermal camera is mounted outside the building chamber enclosing an angle of 45° with the building platform (cf. Figure 1). This angle and a low depth of focus restrict the investigations conducted in this study to a small section of the total building area. Nevertheless, regarding future integration concepts and current developments in thermal detector technology, resolutions of up to 1280 x 960 pixels are feasible giving rise for the observation of the complete building area at the same order of pixel resolution and smaller view angles.
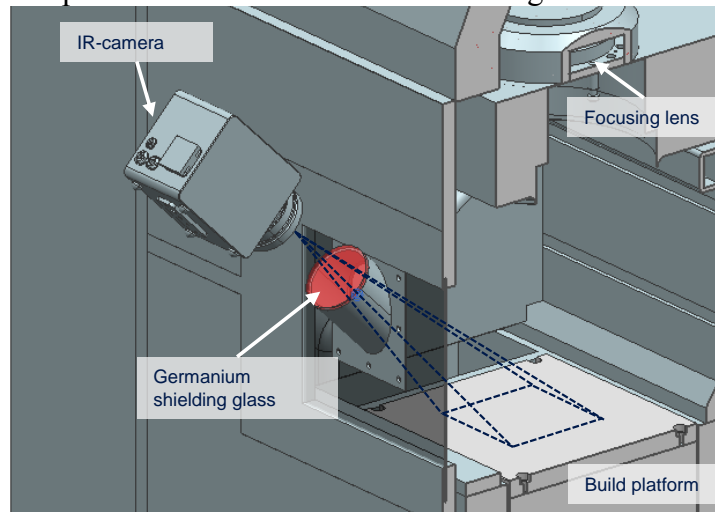

Figure 1:   Experimental setup: IR camera at LWIR wavelength band and 50 Hz sampling rate, 50 mm camera objective, Germanium shielding glass (Transmission > 80%), view angle on building platform: 45°

Compared to commercially available quantum detectors, which are featuring sampling frequencies of multiple kHz, the microbolometer camera utilized in this case has some drawbacks but may potentially provide a cost-effective monitoring solution. The principle of a microbolometer detector is based on the measurement of an increase of resistance due to thermal heating of an absorber material. The indirect measurement of thermal irradiance with uncooled microbolometer detectors therefore implies a typical time constant of 5-15 ms [25] for cool-down purposes leaving an exposure time of typically 5-15 ms when operated at a frequency of 50 Hz. For efficiency purposes the readout of this kind of sensors is done sequentially in a rolling frame mode [25] implying a temporal shift of about 40 µs between subsequent detector lines. To compensate measurement errors, drifts and image inhomogeneities due to parasitic radiation a Non-Uniformity-Correction (NUC) has to be carried out, which interrupts the measurement process for a few milliseconds. These and other restrictions like temporal and spatial crosstalk

---

[3] Long-wavelength infrared

and border pixel issues have to be considered when using microbolometer detectors for monitoring the SLM process.

The determination of absolute temperatures of hot metal surfaces is an ambitious task and practically impossible [9]. Even when assuming a perfect gray body of known emissivity, the rough surface due to aligned single melt tracks leads to imprecise temperature values. Furthermore, emissivity depends on view angle, wavelength and temperature itself which exacerbates the problem of determining the absolute temperature in the heat affected zone with single color pyrometers. Regarding process monitoring of a complete layer one has different states of matter at different temperatures and different emissivities (powder, solidified part and melt). However, the temperature of the unsolidified powder bed and the cooled down solidified part can be approximated.

For the purpose of this paper, the absolute irradiance intensity is taken as the measurement value. This value is proportional to the camera output signal for a preconfigured emissivity value of 1.0 [26]. The use of radiant intensity circumvents the approximation of the absolute temperature and the comparison between different objects (for example powder bed and solidified part) in radiometric terms tends to have less uncertainty. The calculation of the absolute temperature out of this measurement value depends on detector type, calibration setup and the accuracy of emissivity determination, which is not a focus in this paper.

Results and discussion

The conducted investigations on process monitoring focus the detection of parameter deviations during the building process. These can be caused by drifts of process parameters or random process errors. Furthermore the detection of internal cavities and artificial flaws was analyzed. The employed scan strategy is a stripe exposure with a typical scan velocity of 1200 mm/s, a scan vector length of 5 mm, a hatch distance of 90 µm and a focused beam diameter of approx. 80 µm, cf. Figure 2a.
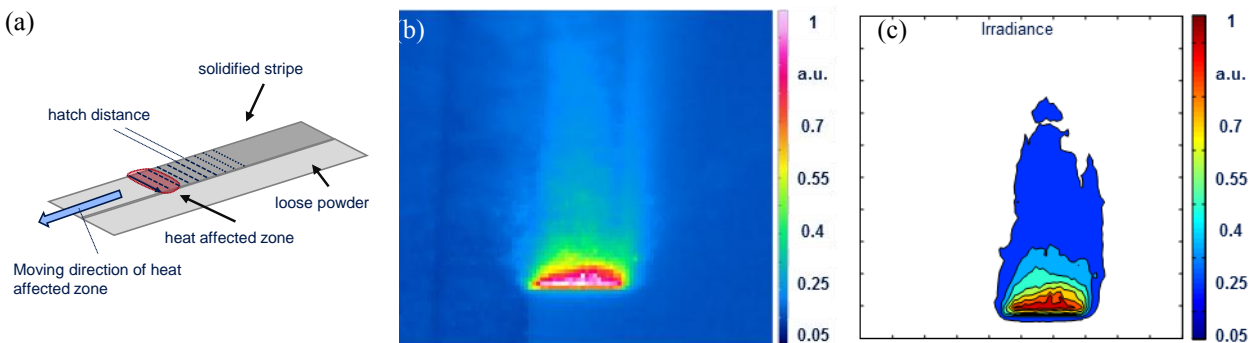

Figure 2: **(a) stripe exposure strategy - qualified process parameters: vector length (stripe width): 5 mm, scan velocity: 1200 mm/s, hatch distance: 90 µm, laser power: 195 W. (b) sample thermogram of the heat affected zone for qualified parameters. (c) areas for different irradiance values**

The microbolometer detector therefore integrates over two complete hatch lines when assuming an integration time of 8 ms and neglecting the dead time between subsequent hatch lines. Therefore, fluctuations of process parameters can only be resolved in the same time domain. For a better comparison of the measurement results all thermograms were taken for a stripe exposure with a moving direction directly towards the IR-camera. A standard deviation for

the considered values was derived from five subsequent thermograms with the heat affected zone being in the center of the focal plane.

Part A: Sensitivity to exposure parameter deviations

Figure 2b shows the heat affected zone during a stripe exposure at typical exposure parameters. The zone moves towards the negative y-axis forming an extended tail on the already solidified area. Part contour and powder bed can be distinguished due to different emissivity values. The melt pool radiance is estimated to be at the order of 6000 a.u. while the maximum radiance recorded here is smaller by a factor of approx. 5. This results from the temporal and spatial integration of a few hatch lines as discussed above. The heat affected zone builds out a bulging towards the powder bed at the border between powder and part because of different heat conductivities. The typical cool down time in terms of irradiance for the given setup is 160 ms (1/e value). Typical irradiance values for different areas of interest are given in Table 1.

	Irradiance [a.u.]	Standard deviation [a.u.]
Maximum in process zone	1.000	0.039
Solidified Area	0.139	0.004
40 μm powder layer on top of solidified area	0.145	0.001
Powder bed	0.127	0.001

Table 1: Irradiance values for different areas of interest

Unlike in other work on similar subjects, the heat affected zone is characterized in terms of the total area, not only for one specific but for multiple irradiance values. The spatial resolution additionally enables the determination of the maximum width and length of the heat affected zone, the aspect ratio and a circularity value. Circularity is a geometry dependent parameter and given by the ratio of the measured area and the area of a circle both having the same perimeter. Figure 3 shows the measured parameters for two different scan velocities. An increase of 16% leads to a significant change in the heat affected area at low irradiance levels. For higher irradiance levels, the difference is in the order of the standard deviation and therefore cannot be determined robustly. The error bars indicate a derogation of a standard deviation.
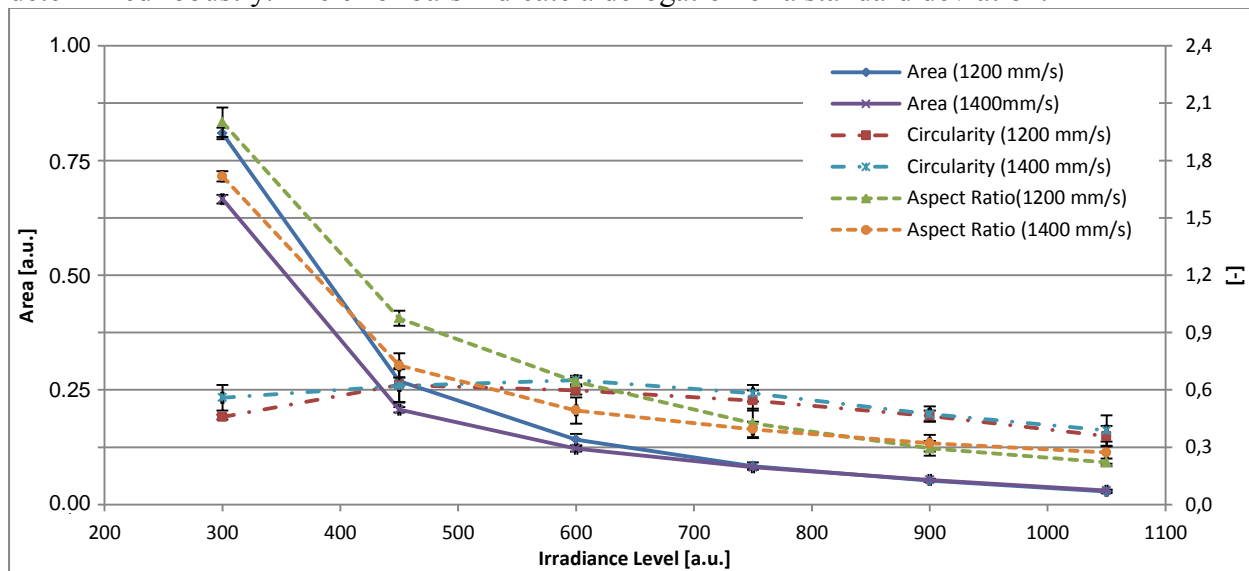

Figure 3:   area, circularity and aspect ratio for different irradiance levels and scan velocities.

The measurement values for a scan velocity variation of ±25% relative to the qualified setting of 1200 m/s are given in Figure 4. Higher scan velocities lead to a significant change of the measured area of the heat affect zone only for low irradiance levels (450 a.u. in this case). At low to medium scan velocities, it can be seen that the effect of decreasing energy input per unit distance is compensated by the increasing number of exposed hatch lines during integration time, resulting in a comparable area size. Nevertheless, it can be concluded that the total area is a suitable variable for detecting scan velocity deviations, when knowing the exact relation or comparing this to a reference value. Circularity and aspect ratio vary in the order of their standard deviation so they may not be used for detecting scan velocity fluctuations.
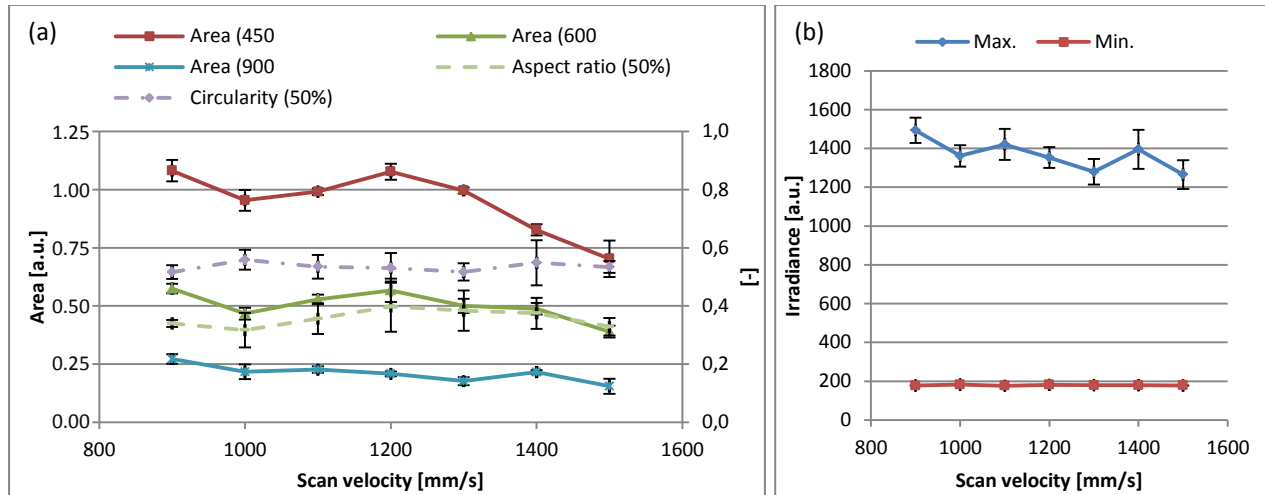

Figure 4: (a) area, aspect ratio and circularity for different scan velocities. (b) maximum and minimum irradiance.

The stability of the laser power is a key factor for high quality, reproducible and dense parts, but can be subjected to fluctuations. These can be caused by pollution of the protective glass, focus shifts due to a temperature increase in the optical components or a laser source malfunction. The detection sensibility of the given setup for a laser power in the rage of 50 W to 195 W can be seen in Figure 5.
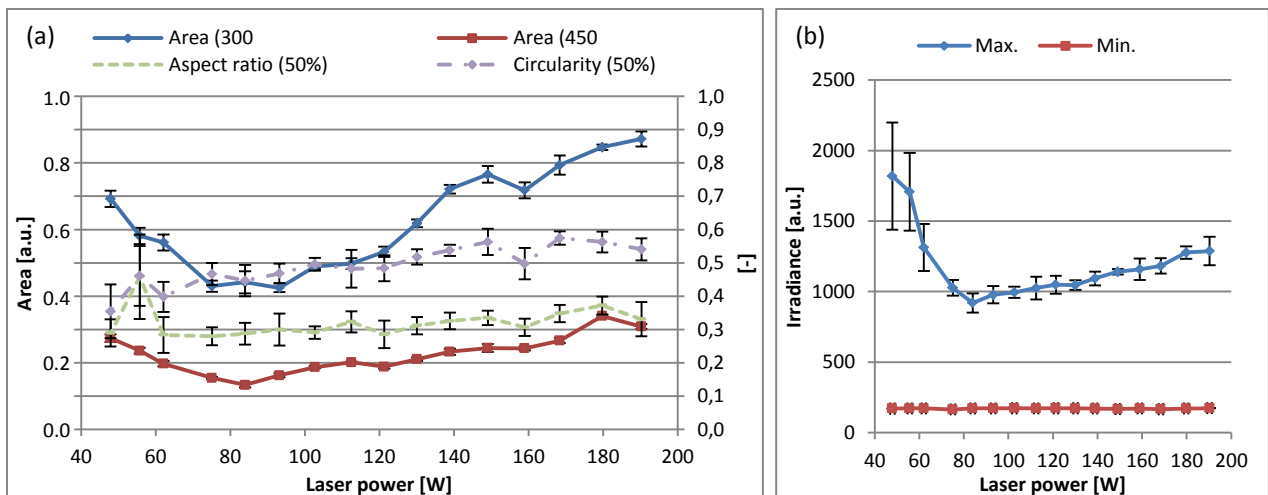

Figure 5: Sensitivity to different laser power values (laser power measured with *Primes Pocketmonitor PMT 05p*. (a) area, aspect ratio and circularity for different irradiance levels. (b) maximum and minimum irradiance.

At a low irradiance level of 300 a.u. deviations of ±10 W can be detected in general. This also holds for medium irradiance levels in the order of 400 a.u. to 800 a.u. but not for the high irradiance levels above 1000 a.u.. As an example, at the irradiance level of 750 a.u. the area of the heat affected zone changes from 5.8 a.u. to 4.9 a.u. when reducing the laser power from 180 W to 170 W, while the standard deviation is 0.2 a.u.. The circularity and the aspect ratio show a weak dependence but can in principle be used for the detection of laser power deviations, knowing that the standard deviation is about 10% of their actual value.

The maximum irradiance value as well as the area of heat affected zone show a monotonic dependency for decreasing laser power values in the range of 200 W to 80 W. For lower laser power, the area and the maximum irradiance significantly rise again. This behavior can be explained by the specific surface structure that results after low energy input. The powder particles are not completely melted and neighboring scan tracks are not connected sufficiently. This results in a deterioration of the heat dissipation and therefore in an increase of the heat affected area. Due to slower dissipation the sampling of the total irradiance becomes more accurate and accounts for higher maximum irradiance levels, whereas the process instabilities account for higher standard deviations.

Other scan strategy parameters that affect the heat up and cool down behavior, and consequently the resulting microstructure include the scan vector length and the hatch distance. An increasing hatch distance will affect the remelting of neighboring single tracks and the metallurgical connection to the latter, while the mean cool down time before remelting occurs is given by the scan vector length. Deviations from preselected values cause the heat affected zone to change its dimensions. The reasons for deviations can be malfunctions or long-term drifts in the scanning subsystem, which are in the sub-millirad range within the state of the art for galvo scanners [27]. This corresponds to a positioning error on the build substrate of 0.2 mm, which can be detected by the spatially resolving off-axis system as long as deviations occur at a timescale longer than milliseconds.

Figure 6 shows the dependency of the heat affected area and other geometrical parameters to deviations of hatch distance out of a sensitivity analysis. For increasing hatch distance the area at low irradiance values decreases significantly and almost monotonous. This also holds for high irradiance values except that the signal to noise ratio in terms of difference in area and standard deviation becomes less.
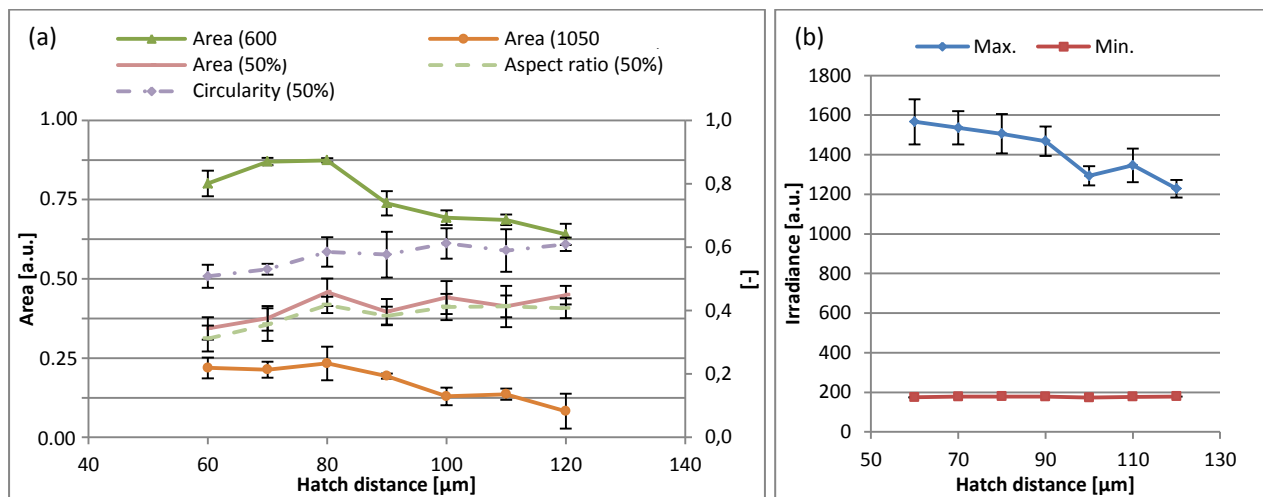

Figure 6: **Sensitivity to different hatch distances. (a) area, aspect ratio and circularity. (b) maximum and minimum irradiance**

The decrease is justified by the fact that at low hatch spacings an overheating takes place which is not compensated by an improved heat dissipation. For greater hatch spacings subsequent hatch lines are physically not connected but the energy input per unit area is less and so is the total area of the heat affected zone. In any case, during the sensor integration time two new hatch lines are exposed and the heat affected zone consists of typically more than four subsequent hatch lines, depending on the chosen irradiance level. Regarding the total area at relative irradiance values (i. e. 50%), there is no significant dependency recognizable. This is clear since the total measured irradiance value also decreases with increasing hatch spacing because total energy is distributed over a greater area for the given integration time (Figure 6b).

The sensitivity to changes of scan vector length is shown in Figure 7. In contrast to the hatch distance dependency, the total area at low irradiance values grows for increasing scan vector length, while the maximum irradiance value decreases monotonously. For longer scan vector lengths the number of single scan tracks observed during camera integration time decreases. Nevertheless, the resulting effect of a shorter longitudinal extent of the heat affected zone is overcompensated by a greater lateral extent corresponding to the chosen scan vector length. This leads to an increase of the total heat affected area. Unlike in hatch spacing dependency, the aspect ratio and circularity parameter measured for increasing scan vector lengths show a rapid decrease while being subjected to considerable fluctuations in both cases.
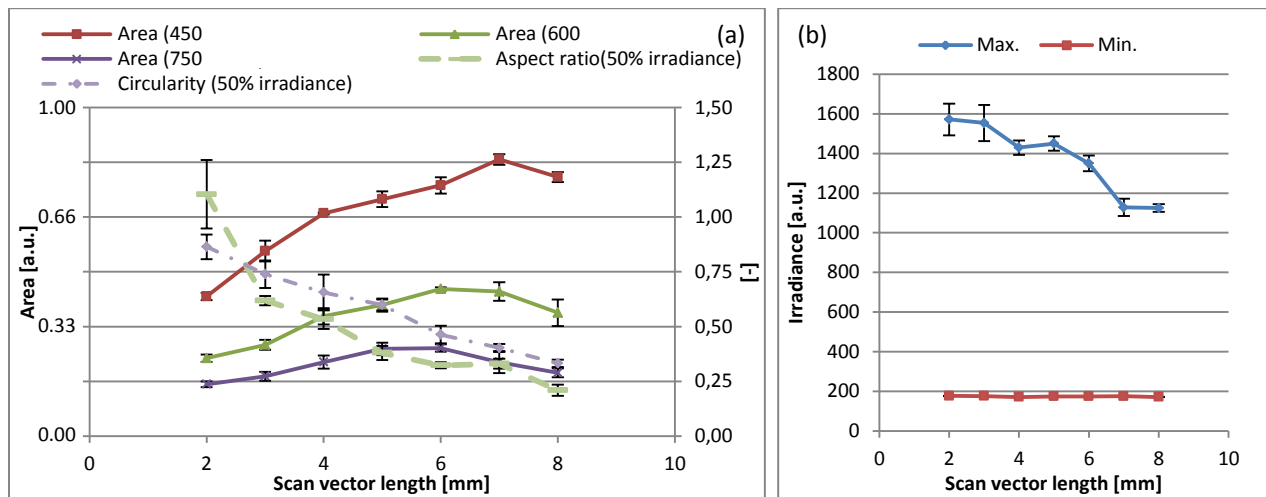

Figure 7: **Sensitivity to different scan vector lengths. (a) area, aspect ratio and circularity. (b) maximum and minimum irradiance**

For industrial applications it can be concluded that variations due to scanning issues can be detected when the resulting positioning errors accumulate over multiple scan tracks. This is reasoned by the limited integration time of the given setup. Furthermore all the considered process parameter deviations have to occur at a spatial extent of square millimeters to be detectable by this setup, since the total area of the heat affected zone that is used as measurement variable has this order of magnitude.

Part B: Sensitivity to artificial flaws/pores

Material defects such as pores, cavities or cracks are likely to occur in any layerwise build up process. Depending on their size and geometrical shape they can be relevant for a later part failure. Varying powder layer thickness is typically encountered at overhanging structures or caused by inhomogeneous coating, both giving rise for possible process errors. Differences in the

powder layer thickness can be detected during the solidification process, which is shown in Figure 8 for a stripe exposure strategy. The total area at all investigated irradiance levels increases almost monotonously with growing layer thickness. This is caused by a melt pool enlargement due to low heat conductivity. As can be seen from Figure 8b the measured maximum irradiance values also increase. This can be explained by the extended solidification time which causes the sampling of total irradiance to become more accurate.
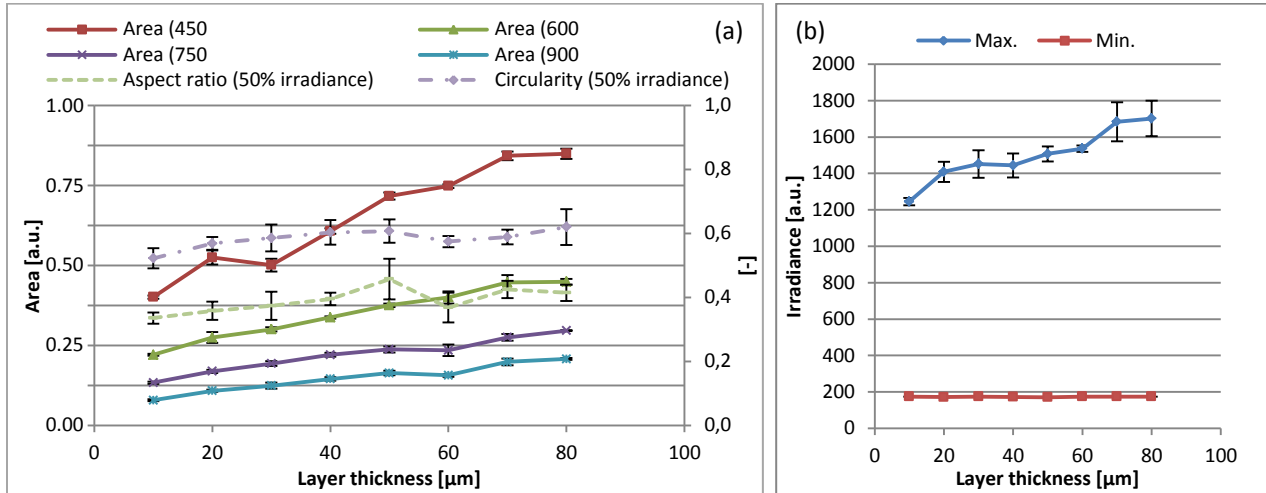

Figure 8: Sensitivity to different layer thicknesses. (a) area, aspect ratio and circularity. (b) maximum and minimum irradiance

In the subsequent part, artificial flaws and their detectability with the given thermography system are investigated. Artificial flaws were created by omitting certain round-shaped areas during exposure of multiple subsequent layers. This results in cavities that are filled with loose powder after recoating. After a specific number of layers corresponding to a total flaw height the next layer was completely solidified. This causes a sealing of the underlying loose powder which represents the artificial flaw (Figure 9). The total dimension, contour and shape of the flaws depend on the accuracy of the machine beam offset value and are subjected to the agglomeration and the adhesion of additional powder particles, so the given dimensions are only nominal values.
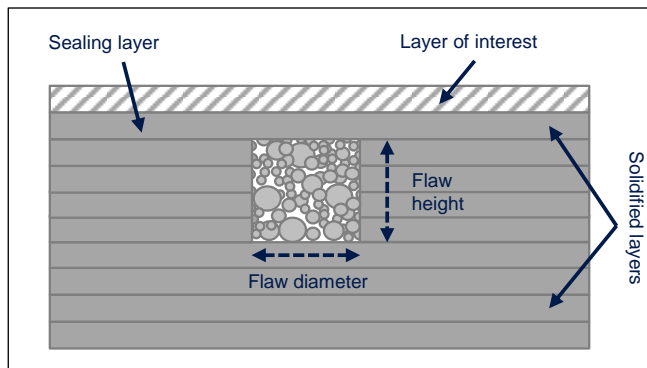

Figure 9: Artificial flaw. The layer of interest is the first layer after the sealing layer.

The detection of flaws was conducted by measurements of the temporal evolution and the spatial distribution of the total irradiance during exposure of a new layer. Figure 10a shows the spatial irradiance distribution in the region of an artificial flaw, 120 ms after the exposure of the

1009

flaw. In the left-hand part of the figure the dark area corresponds to an already solidified zone, whereas the right-hand side represents loose powder. The heat affected zone moves downwards for proceeding exposure process leaving an area of increased irradiance at the flaw site. This can be clearly identified when regarding the irradiance on a line-profile, as it is shown in Figure 10b for a flaw of 300 µm diameter and 140 µm height. A bossing forms after the main peak which can be characterized in terms of its difference to a reference profile. This reference profile was derived from non-flaw exposures and shows standard deviations of the order of 15% at the peak location. The tail (cool-down area) of such line profiles reveals characteristic distortions due to the resulting surface structure of the solidified area and accounts for approx. 5% standard deviation in the reference profile.
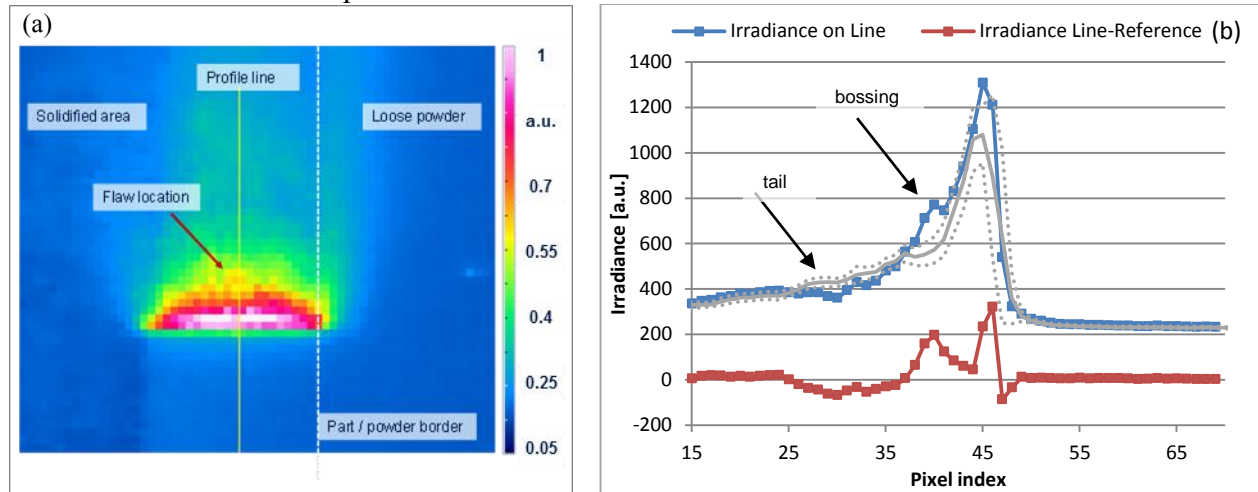

Figure 10 (a) thermogram of heat affected zone after passing of artificial flaw. (b) corresponding irradiance for line profile, reference for non-flaw exposure including standard deviation (dotted line) and difference between both.

In Figure 11a the maximum irradiance difference between flaw site and reference is shown for different flaw sizes. The specific time offset between exposure of the flaw and recording of the thermogram was chosen in a way to get a maximum visibility of the resulting signal.

As expected, this difference decreases for decreasing flaw sizes (diameter and height). Furthermore the minimal flaw size that can be detected is indicated as the difference tends to become negative. This corresponds to a signal that has no significant bossing, which is the case for flaws of linear dimension < 100 µm. Nevertheless, a hint indicating the existence of flaws smaller than this limit is the significantly lower irradiance in the tail section of the measured profiles (Figure 11b). This is observed for all the considered flaws.

The analysis in terms of temporal evolution is shown in Figure 12. The maximum irradiance at the specific flaw location tends to become less with decreasing flaw height, whereas the peak full width at half maximum (FWHM) shows no characteristic dependency. The absolute value of peak width indicates however the existence of irregularities and flaws. Its difference to the reference peak width is greater by one order of magnitude compared to the standard deviation as can be seen from Figure 12b for a flaw diameter of 300 µm and flaw height of 140 µm. From this results it can be concluded, that the peak height as well as peak width is an indicator for existing flaws in the investigated flaw size range of $0.4 \cdot 10^{-3}$ mm³ to $100 \cdot 10^{-3}$ mm³. Nevertheless, the identification robustness is subjected to considerable fluctuations in total irradiance and therefore in the peak FWHM.
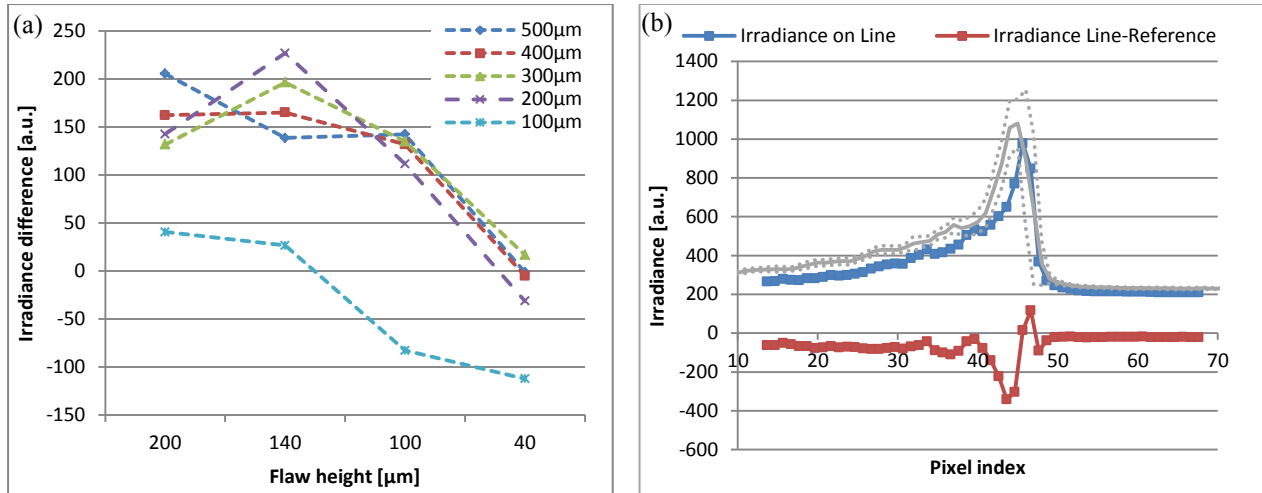
Figure 11: (a) difference in irradiance for different flaw sizes. (b) irradiance profile for a shallow flaw.
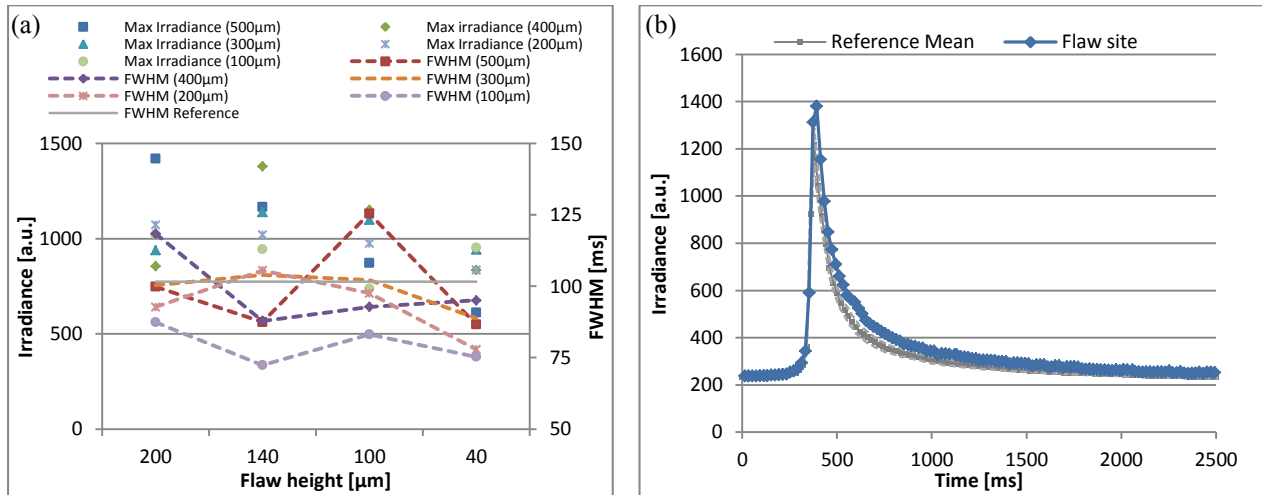

Figure 12: (a) maximum irradiance and FWHM for different flaw sizes in time domain. (b) temporal evolution of irradiance for flaw (300 μm diameter, 140 μm height) and reference curve.

Conclusion and Future Work

Monitoring the SLM process by using thermography is a promising approach for the complete documentation of the layerwise build-up process. A cost efficient bolometer camera has been set up for monitoring the SLM process and its sensitivity to detect process deviations was investigated. Assuming that deviations occur at a timescale greater than 20 ms, they can be detected through comparing different measurement results to predefined reference values. As characteristic quantities the total area of the heat affected zone at specific irradiance values as well as the circularity and the aspect ratio were investigated. It can be concluded that the total area is a good indicator for process parameter deviations whereas the circularity and the aspect ratio can be used to detect deviations and drifts in the scanning unit when scan vector length and scan vector spacing (hatch distance) are affected.

Furthermore, the detection of artificial flaws in the range of 40 μm to 500 μm was analyzed. The order of magnitude corresponds to the spatial resolution of the given setup of approx. 250 μm. By examination of the spatial irradiance distribution at flaw site shortly after the

exposure and its temporal evolution during solidification, flaws could be identified up to a size of 100 μm. The artificial flaws induced here show a decelerated cool down characteristic because of lower heat conductibility.

Future work will focus on the correlation between process parameter deviations and resulting material properties as well as alternative camera integration concepts to allow for a smaller view angle. Because of limitations due to the chosen view angle, the analysis in this paper was done for an area close to the center of the building platform within the camera focus. The reference values depend on the movement direction of the current process zone and were calculated for the special case of a camera-approaching heat affected zone. This limitation has to be overcome in future to be able to monitor the complete build area and to account for its inhomogeneity.

The benefit of using an off axial thermography setup at a fixed location is the possibility to monitor the actual solidification process as well as the quality of powder layer deposition without the need for additional illumination. Thermography opens up for detecting differences in powder layer thickness directly after recoating. Since the regions of less powder height are heated up more quickly to the temperature of the underlying solidified zone, they can be distinguished from areas of higher powder layer thickness. Because of the low heat conductivity of metal powders, this takes place at the timescale of milliseconds, which is easily detectable by bolometer cameras. The detection of coater wear and insufficient powder coating will be subject of future work. Additionally the advantage of using thermography equipment with higher temporal and spatial resolution will be investigated.

Acknowledgment

References

[1]   Zäh, M. (Editor): Wirtschaftliche Fertigung mit Rapid-Technologien. München, Wien: Hanser 2005. ISBN: 3446228543.

[2]   Kruth, J.-P.: On-line monitoring and process control in selective laser melting and laser cutting. In: M. Geiger et al. (Editor): Proceedings of the 5th Lane Conference, Laser Assisted Net Shape Engineering 2007, pp. 23-37.

[3]   Craeghs, T.; Clijsters, S.; Yasa, E.; Bechmann, F.; Berumen, S.; Kruth, J.-P.: Determination of geometrical factors in Layerwise Laser Melting using optical process monitoring. Optics and Lasers in Engineering 49 (2011) 12, pp. 1440-1446.

[4]   Craeghs T.; Clijsters S.; Yasa E.; Kruth J.-P.: Online quality control of selective laser melting. In: Bourell, D. (Editor): Solid Freeform Fabrication: Proceedings, August 2011: University of Texas at Austin 2011.

[5]   Craeghs, T.; Bechmann, F.; Berumen, S.; Kruth, J.-P.: Feedback control of Layerwise Laser Melting using optical sensors. Physics Procedia 5 (2010), pp. 505-514.

[6]   Berumen, S.; Bechmann, F.; Lindner, S.; Kruth, J.-P.; Craeghs, T.: Quality control of laser- and powder bed-based Additive Manufacturing (AM) technologies. Physics Procedia 5 (2010), pp. 617-622.

[7]   Bechmann, F.; Berumen, S.; Craeghs, T.; Clijsters, S.: Prozessüberwachung und Qualitätssicherung generativ gefertigter Bauteile. In: Fraunhofer Additive Manufacturing Alliance (Editor): Direct Digital Manufacturing Conference 2012. Berlin, March 14-15, 2012.

[8]   Lott, P.; Schleifenbaum, H.; Meiners, W.; Wissenbach, K.; Hinke, C.; Bültmann, Jan: Design of an Optical system for the In Situ Process Monitoring of Selective Laser Melting (SLM). Physics Procedia 12 (2011), pp. 683-690.

[9]   Bayle, F.; Doubenskaia, M.: Selective laser melting process monitoring with high speed infra-red camera and pyrometer. (Editor): Proceedings of SPIE: SPIE 2008, pp. 698505-698505-8.

[10]   Chivel, Y.; Smurov, I.: On-line temperature monitoring in selective laser sintering/melting. Physics Procedia 5 (2010), pp. 515-521.

[11]   Ljungblad U.: Process Surveillance in Electron Beam Melting for Cost-Efficient Production of Complex Parts. In: Fraunhofer Additive Manufacturing Alliance (Editor): Direct Digital Manufacturing Conference 2012. Berlin, March 14-15, 2012.

[12]   Schwerdtfeger J.; Singer R.; Körner C.: In-situ Flaw Detection by IR-imaging during Electron Beam Melting. Rapid Prototyping Journal (2012) 18.

[13]   Wegner, A.; Witt, G.: Process Monitoring in Laser Sintering using Thermal Imaging. In: Bourell, D. (Editor): Solid Freeform Fabrication: Proceedings, August 2011: University of Texas at Austin 2011.

[14]   Wegner, A.; Witt, G.: Thermographie zur Temperaturmessung beim Laser-Sintern – ein Beitrag zur Qualitätssicherung? RTejournal - Forum für Rapid Technologie (2011) 8.

[15]   Schutzrecht EP 1 466 718 B1 (15.06.2011) 13.10.2004. Chung, M.: Sintering method and apparatus using thermal image feedback.

[16]   Schutzrecht DE102007056984A1. EOS GmbH Electro Optical Systems. 27.11.2007 Philippi, J.; Mattes, T.: Verfahren zum Herstellen eines dreidimensionalen Objektes mittels Lasersintern.

[17]   Stache, N. C.; Zimmer, H.; Gedicke, J.; Olowinsky, A.; Aach, T.: Robust high-speed melt pool measurements for laser welding with sputter detection capability. In: Hamprecht, F. A. et al. (Editor): Pattern recognition. Berlin, New York: Springer 2007, pp. 476-485. ISBN: 3540749330.

[18]   Stehr, T.; Hermsdorf, J.; Henning, T.; Kling, R.: Closed loop control for laser micro spot welding using fast pyrometer systems. Physics Procedia 5 (2010), pp. 465-471.

[19]   Bartkowiak, K.: Direct laser deposition process within spectrographic analysis in situ. Physics Procedia 5 (2010), pp. 623-629.

[20]   Dietrich, S.: Sensoriken zur Schwerpunktslagebestimmung der optischen Prozess-emissionen beim Laserstrahltiefschweißen. Bamberg: Meisenbach 2009. ISBN: 3875252926.

[21] Kolossov, S.; Boillat, E.; Glardon, R.; Fischer, P.; Locher, M.: 3D FE simulation for temperature evolution in the selective laser sintering process. International Journal of Machine Tools and Manufacture 44 (2004) 2-3, pp. 117-123.

[22] Branner, G.: Modellierung transienter Effekte in der Struktursimulation von Schichtbauverfahren. München: Utz 2011. ISBN: 978-3-8316-4071-3.

[23] Patil, R. B.; Yadava, V.: Finite element analysis of temperature distribution in single metallic powder layer during metal laser sintering. International Journal of Machine Tools and Manufacture 47 (2007) 7-8, pp. 1069-1080.

[24] Pottlacher, G.; Hosaeus, H.; Wilthan, B.; Kaschnitz, E.; Seifter, A.: Thermophysikalische Eigenschaften von festem und flüssigem Inconel 718. Thermochimica Acta 382 (2002) 1-2, pp. 255-267.

[25] Sackewitz, Michael (Editor): Leitfaden zur Wärmefluss-Thermographie. Stuttgart: Fraunhofer-Verlag 2011. ISBN: 9783839602348.

[26] FLIR Systems A. B.: The Ultimate Infrared Handbook for R&D Professionals. <http://www.flir.com/uploadedFiles/Thermography/MMC/Brochures/T559243/T559243_EN.pdf> - 27.06.2012.

[27] SCANLAB AG: hurrySCAN ®, hurrySCAN ® II datasheet. <http://www.scanlab.de/link/de/49473> - 02.07.2012.